Alexandria Journal of Science and Technology

Article

Optimization of the Steel Casting Process Parameters to Control the Longitudinal Facial Crack (LFC) Defect Appearance

Magdy, T. Feshar [1], Fatma, M. Mahgoub [1, *], Ashraf, M. Abdel-Gaber [2]

[1] *Institute of Graduate Studies and Research, Materials Science Department, Alexandria University, 21526 Alexandria, Egypt. Email: ftm_mahgoub@alexu.edu.eg.*

[2] *Chemistry Department, Faculty of Science, Alexandria University, 21321 Alexandria, Egypt. Email: ashrafmoustafa@yahoo.com.*

[*] *Correspondence Address:*

Fatma, M. Mahgoub: Institute of Graduate Studies and Research, Materials Science Department, Alexandria University, 21526 Alexandria, Egypt. Email: ftm_mahgoub@alexu.edu.eg.

KEYWORDS: LFC; SEM; Electrochemical Techniques; Heat Flux; Mould Flux; Non-metallic Inclusion.

Received:
October 10, 2023
Accepted:
December 23, 2023
Published:
January 04, 2024

ABSTRACT: The principal aim of this research is to meticulously detect and comprehend the reasons behind the longitudinal facial crack (LFC) defect during the casting of low-carbon, low-manganese flat steel products. The overarching goal is to mitigate the likelihood of the defect occurring by optimizing key process parameters. Even seemingly minor defects are considered unfavorable in the final product due to the substantial manufacturing losses entailing economic repercussions.

The research employs a diverse array of techniques, including the utilization of a scanning electron microscope (SEM), energy-dispersive X-ray spectroscopy (EDX), potentiodynamic polarization curve measurements, and electrochemical impedance spectroscopy (EIS) measurements. LFC defect samples undergo electrochemical testing, with comparisons made against a control sample. Additionally, selected LFC samples undergo scrutiny using SEM and EDX under varying process parameters, including carbon equivalent percentage, isostatic flow control material, non-metallic inclusions, and mold flux. Findings underscore that optimizing key process parameters in both the thin slab caster and the melt shop effectively diminishes the occurrence of LFC defects. Manipulating these factors proves

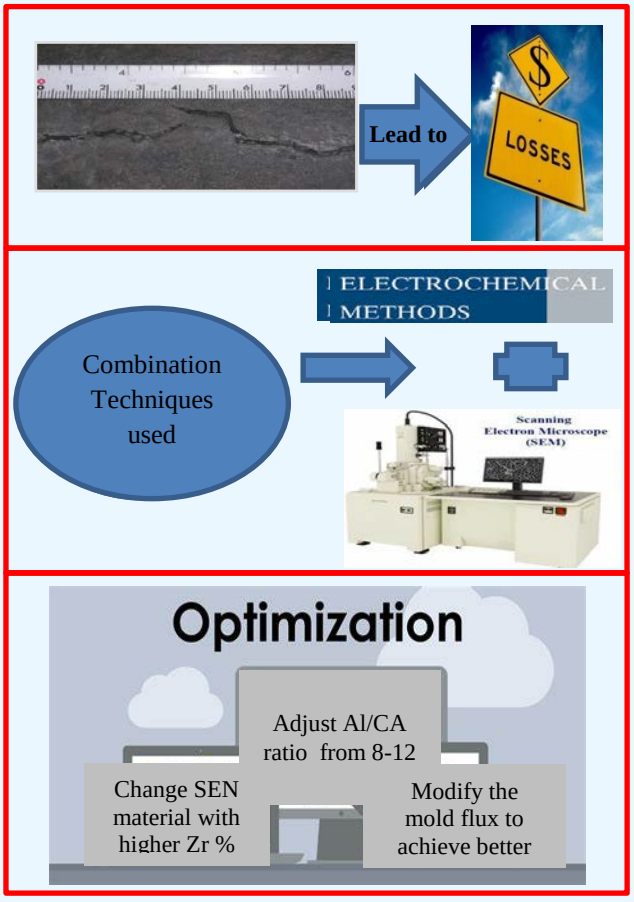

Online ISSN: 2974-3273

DOI: 10.21608/ajst.2024.333736

instrumental in reducing the frequency of LFC defects, consequently minimizing economic costs associated with the reproduction of defective products. Potentiodynamic polarization curve measurements reveal that the isostatic flow parameter significantly inhibits the corrosion of the LFC sample. In contrast, other parameters contribute to the manifestation of corrosion in the LFC defect. A carbon equivalent exceeding 0.065% results in a heightened corrosion rate, whereas non-metallic inclusions exhibit the lowest corrosion rate. Electrochemical impedance spectroscopy (EIS) measurements demonstrate that the sample subjected to isostatic flow control in 0.5 M NaCl exhibits the highest corrosion resistance (highest Rmin), while other parameters contribute to an acceleration in the corrosion rate. Identification and resolution of fundamental causes involve strategic adjustments, such as adapting the carbon equivalent percentage to be less than or equal to 0.065% to decrease the likelihood of density changes during the "δ -> γ" transformation. This transformation induces mechanical stress increases in the shell. Additionally, altering the isostatic flow control material, especially increasing zirconia to 92% from 85%, aims to decrease erosion rates. Controlling non-metallic inclusions during the ladle metallurgical process by adjusting the aluminum to calcium ratio to fall within 8 to 12, and adapting mold flux chemical and physical properties, such as increasing basicity from 1.01 to 1.05 while decreasing viscosity from 0.90 to 0.80 Poise, contribute to overall improvements in production and efficiency. Consequently, the financial and environmental costs associated with manufacturing defective products are substantially reduced.

1. INTRODCTION

The implementation of compact strip production (CSP) as a method for generating hot rolled coils significantly improves both quality and energy efficiency. Introduced in 1989 and continually evolving, CSP is widely recognized as a successful manufacturing approach [1]. While CSP achieves the highest level of internal quality compared to conventional thick slab methods, it is more susceptible to the longitudinal facial crack (LFC) defect [3]. CSP relies on a continuous and integrated casting machine, coupled with a reheating furnace and a hot strip mill line, to meet specific material specifications based on customer requirements [2]. In contrast, thin slab production involves the use of a specialized mold with a funnel shape, requiring robust indirect water cooling for primary solidification. The transition zone from the mold funnel region to the parallel section introduces more stress, leading to a higher cracking index in the transition region of CSP thin slabs compared to conventional slab production [2-4]. The mold, influenced by complex process parameters such as mold flux for lubrication and mold cooling water, is considered a major contributor to various slab quality issues, particularly in meniscus areas [5]. LFC defects tend to occur at different locations across the slab width, often concentrated toward the slab center with varying degrees of severity [6]. Several mechanisms have been developed to illustrate the primary causes of the formation of longitudinal facial cracks (LFC) defects. These mechanisms are directly linked to the generation of tensile stress surpassing the fracture strength of steel, particularly at elevated temperatures. Additionally, changes in the physical and chemical properties of mold flux, along with the non-uniformity of heat flux due to the thermomechanical behavior of the slab inside the mold, contribute to defect formation [7,8,9]. The stress generation leading to LFC defects can result from thermal stress due to free expansion or contraction, as well as mechanical stress arising from inadequate mold flux lubrication or malfunctioning mold taper causing mold and slab fraction [6,7,8]. Numerous metallurgical factors, including the presence of a low ductility zone, have been identified as contributors to the formation of LFC in the strand shell. Specifically, the existence of a low ductility zone in steel above 1340°C has been demonstrated to influence the appearance of LFC defects [10]. Extensive research indicates that various process parameters play a significant role in the occurrence of LFC defects. Several research studies have delved into the examination of surface longitudinal cracks on SPA-H steel slabs produced through CSP. These investigations have highlighted the notable impact of fluctuations in aluminum content on mold powder composition and slab surface quality. This effect becomes particularly significant when there are variations in molten steel superheat or when titanium is introduced to the molten steel [5]. Additionally, other studies have explored a range of casting parameters, including heat transfer, steel superheat, casting speed, secondary cooling water, Mn/S ratio, and chemical composition. These parameters were investigated to address longitudinal cracks in thicker slabs produced by a Conventional Caster at low casting speeds, capped at a maximum of 2 m/min[5]. In addressing cracks formed primarily at the slab corner due to the addition of chromium and boron, a study focused on cooling adjustments. Through this approach, the occurrence of cracks was markedly decreased. Furthermore, efforts were made to mitigate the risk of longitudinal surface cracks by examining the relationship between wear profiles of narrow face molds and crack occurrence. This study revealed that wear was more pronounced on the narrow face mold, leading to a reduction in narrow face taper, thus contributing to a reduction in crack occurrence [23]. The current research is focused on different process parameters encompass carbon equivalent, heat transfer (heat flux), non-metallic inclusion content, steel superheat, casting speed variation, secondary cooling water, mold narrow side wear profile, mold taper adjustment, Mn/S ratio, and chemical composition. These factors have been shown to exert a substantial influence on the appearance of LFC defects during the casting process [11].

Finally, the longitudinal facial crack (LFC) defect is observed at various locations along the width of the slab, exhibiting varying degrees of severity. Adjusting carbon equivalent values and fine-tuning mold flux properties has resulted in a reduction of the LFC index. To enhance product quality, attention is directed towards adjusting the Al/Ca ratio at the ladle metallurgy furnace (LMF) to fall within the specified range of 8-12. Electrochemical techniques have revealed that an isostatic flow parameter of 2.6 tons/minute effectively inhibits the corrosion of LFC samples. However, it is noteworthy that other parameters, including non-metallic inclusions, mold flux, and carbon equivalent, contribute to the induction of corrosion in the LFC defect. This study is of considerable importance to the steel industry, representing a pioneering initiative that integrates electrochemical techniques with scanning electron microscopy to enhance industrial processes. The unique combination of these methods marks a groundbreaking advancement in the field, as it has been applied for the first time. The research methodology begins with conducting experimental work that includes potentiodynamic and electrochemical impedance spectroscopy (EIS) measurements. Following this, the study advances to metallographic testing, and a comprehensive discussion of the results is undertaken, considering different process parameters.

2. Results and Discussion

2.1. Investigation of Process Parameters

2.1.1 Carbon equivalent parameter

The carbon equivalent (Ceq) is a crucial weight percentage utilized for evaluating the initial solidification structure and is pivotal in determining the likelihood of cracking. Equation 1 provides a means to calculate Ceq:

$$Ceq = [\%C] + 0.02\,[\%Mn] + 0.04\,[\%Ni] - 0.10\,[\%Si] - 0.04\,[\%Cr] - 0.10\,[\%Mo]. \quad (1)$$

The elemental composition necessary for the carbon equivalent calculation is identified using an optical emission spectrometer (Spectro Ametek, Germany). Table 1 displays the calculated carbon equivalent and LFC index for various samples. According to the data in Table 1, a carbon equivalent percentage exceeding 0.065% can lead to severe LFC, as illustrated in the SEM photo in **Figure 1a**. This suggests a high likelihood of density changes during the delta phase (body-centered cubic structure) to gamma phase (face-centered cubic structure) "δ -> γ" transformation, causing increased mechanical stress in the shell [2,12]. **Figure 1b** demonstrates that a slightly higher Ceq, just above 0.065%, results in only mild LFC. To completely prevent LFC, the carbon equivalent percentage must be equal to or less than 0.065% (**Figure 1C**).

Prior investigations focused on MnS precipitation have uncovered that accumulations of sulfur (S) and phosphorus (P) in interdendritic liquid play a pivotal role in reducing the liquid's freezing temperature. Specifically, the carbon content present in steel emerges as a significant factor influencing the interdendritic segregation of phosphorus. Notably, when the carbon content surpasses 0.1%, there is a pronounced tendency for internal cracks to develop. This propensity is attributed to the occurrence of the austenitic phase during the solidification process[24]. Looking ahead to future research endeavors, there is a promising avenue for studying the tuning or addition of new elements to enhance the overall performance of the steel production process. This exploration could extend to the development of innovative techniques aimed at producing steel grades with higher carbon equivalent percentages, surpassing the threshold of 0.065%.

2.1.2 Submerged Entry Nozzle (SEN) Material

In the current casting process, a submerged entry nozzle (SEN) is employed to convey high-quality molten steel from the tundish to the mold. The SEN, typically constructed from corrosion-resistant materials like alumina (Al2O3) and zirconia (Zr), experiences degradation over time during casting, resulting in a reduction in thickness from 26 mm to 7 mm. **Figure 2** illustrates the Energy Dispersive X-Ray (EDX) results of a sample with an LFC defect, revealing the presence of zirconia components. The significant erosion rate observed during casting, coupled with the zirconia content being exclusive to the SEN material, suggests a malfunction in the material.

To address this issue, the zirconia content in the SEN material has been increased from 85% to 92%, aiming to improve thickness reduction to 15 mm instead of 7 mm. Zirconia is commonly employed to shield submerged entry nozzles (SENs) from corrosion caused by mold slag during the continuous casting of steel [13].

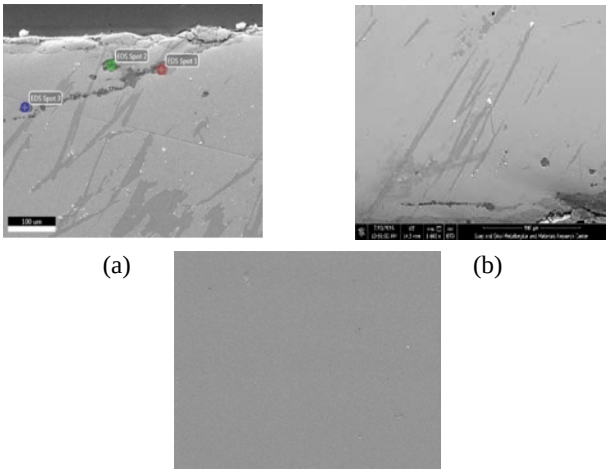

Figure 1. SEM photo for carbon equivalent samples of Ceq (a) > 0.65, (b) ≈ 0.65, and (c) < 0.065.

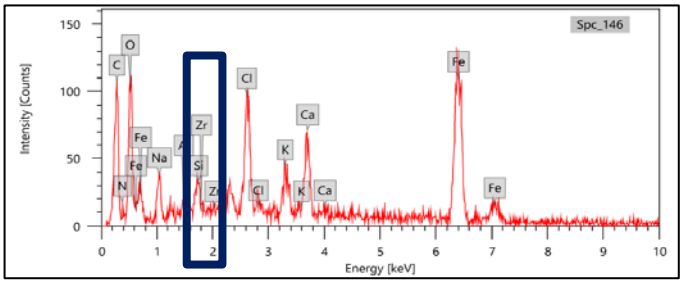

Figure 2. EDX analysis of LFC sample with zirconia content of 85%

Table 1: Carbon equivalent percentage values for different samples

Item %	Percentage %								
Carbon	0.045	0.055	0.065	0.065	0.067	0.055	0.045	0.065	0.055
Manganese	1.200	1.300	1.400	1.400	1.400	1.200	1.200	1.200	1.200
Nickle	0.100	0.100	0.100	0.100	0.100	0.150	0.150	0.100	0.100
Silicon	0.150	0.250	0.250	0.355	0.200	0.355	0.355	0.150	0.250
Chromium	0.100	0.100	0.100	0.100	0.100	0.100	0.100	0.100	0.100
Molybdenum	0.003	0.005	0.005	0.005	0.004	0.003	0.003	0.004	0.003
Carbon Equivalent	0.057	0.055	0.067	0.057	0.074	0.067	0.057	0.073	0.055
LFC index	NO LFC	NO LFC	Light LFC	NO LFC	High LFC	Light LFC	NO LFC	High LFC	NO LFC

2.1.3 Non-Metallic Inclusion (NMI)

Non-metallic inclusions pose a significant quality challenge that can lead to costly casting repairs or the rejection of coils [15, 16]. Elevated levels of total oxygen ppm post-solidification may alter the physical properties of mold flow, resulting in a higher crack index. Examination of LFC samples through SEM (**Figure 3**) and DEX (**Figure 4**) analyses unveiled the presence of non-metallic inclusions (NMIs) like Al_2O_3, CaO, and MgO surrounding the crack defect. High concentrations of sulfur, calcium, and aluminum components were identified, indicating the need for an inspection of the ladle metallurgical furnace.

Preventing this issue involves maintaining clean steel and ensuring sufficient Ca-treatment. This treatment transforms solid Al_2O_3 particles into liquid calcium aluminates, facilitating easier separation and preventing deposition in the flow channel [14, 16]. Following the CaO-Al_2O_3 binary phase diagram, the required amount of Ca varies based on aluminum and oxygen levels. Data analysis indicated that the Al/Ca ratio for the majority of defective heats was either above 12 or below 8. Consequently, reducing the Al/Ca ratio to the range of 8-12 can contribute to a reduction in cracking [16].

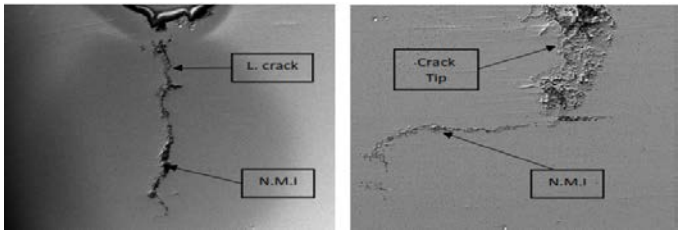

Figure 3. SEM photo for the nonmetallic inclusion near to LFC region.

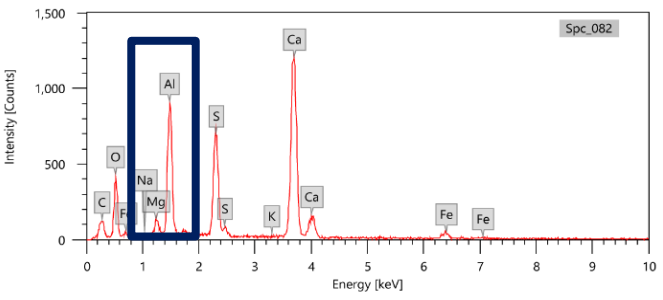

Figure 4. EDX analysis for the nonmetallic inclusions near to LFC.

2.1.4 Mold Flux

Mold fluxes play a pivotal role. These powders are introduced onto the top surface of the molten metal [17]. Three distinct layers are formed: sintered, mushy, and ultimately liquid flux. The liquid slag from the molten pool infiltrates the mold/strand channel, providing lubrication to the newly formed steel shell. For LFC samples, SEM and EDX analyses were conducted. The results revealed the presence of elements such as Ca, Si, Mg, Na, C, F, and Mn, characteristic of mold flux [18]. It is crucial to modify the mold flux to achieve lower viscosity, ensuring improved lubrication and mandating higher basicity for enhanced heat transfer. This, in turn, reduces overall heat transfer and subsequently decreases the crack index [19]. As indicated in the table 2, the basicity increases from 1.01 to 1.05, determined through XRF analysis, while viscosity decreases from 0.90 to 0.80 Poise, measured using the Concentric Cylinder Method [21].

inadequate slag smelting as key factors. Stress concentration,

coupled with thermal stress and mold friction, contributed to cracking. The role of mold powder composition and heat transfer, including calcium silicate and Na, was emphasized. Statistical analysis indicated P, S, Mn, and Mn/S were not primary causes; instead, aluminum content fluctuations played a significant role.

Table 2: Comparison between original mold flux and modified flux

Mold flux type	Basicity (CaO/SiO_2)	Viscosity (at 1300 °C) Poise
Original	1.01	0.90
Modified	1.05	0.80

2.2 Potentiodynamic polarization curves measurements:

Figure 5 depicts the polarization curves of samples, with and without cracks. The presence of cracks can either expedite the cathodic process (sample 3) or the anodic process (samples 1 and 4). Sample 2 shows a slight acceleration in the anodic process but a significant deceleration in the cathodic process. This indicates that cracks influence both the cathodic and anodic reactions associated with corrosion.

Table 3 presents the polarization parameters, including corrosion current density (i_{corr}), corrosion potential (E_{corr}), anodic and cathodic Tafel slopes (βa, βc), determined through the use of Gamry Echem analyst software. The data elucidate that the isostatic flow parameter of 2.6 tons/minute effectively inhibits the corrosion of the LFC sample. Conversely, other parameters contribute to the manifestation of corrosion in the

LFC defect. A carbon equivalent exceeding 0.065 % results in a higher corrosion rate, while non-metallic inclusions exhibit the lowest corrosion rate.

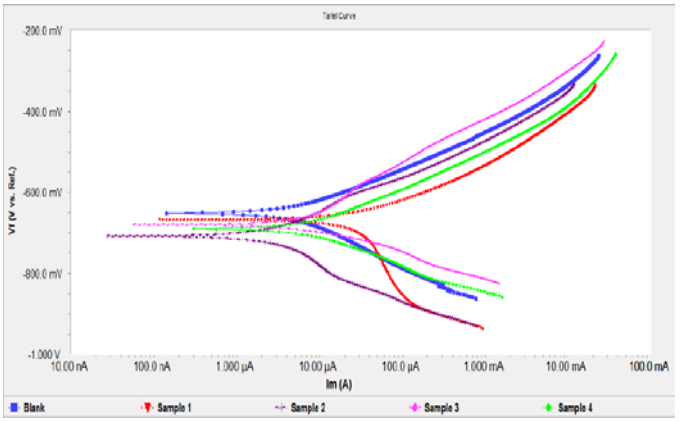

Figure 5. Potentiodynamic polarization curves for five steel samples.

2.3. Electrochemical impedance spectroscopy (EIS) measurements:

Figure 6 shows the Nyquist impedance plots of the blank and LFC samples. The figure shows the impedance response consists of depressed semicircles followed by diffusion tail. This explains that the corrosion process occurs under diffusion control.

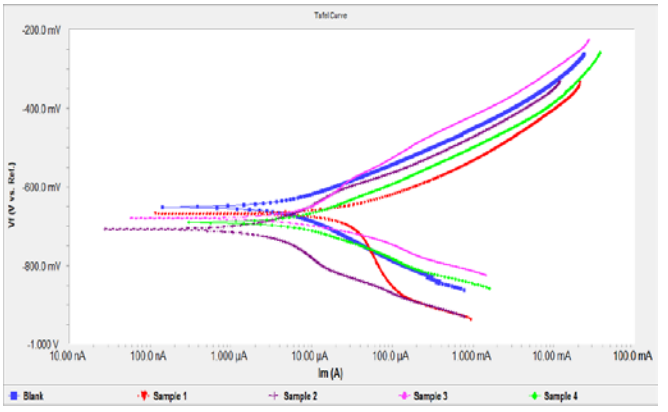

Figure 6. Nyquist Impedance plots for the steel samples.

Figure 7 presents Bode and theta impedance plots for a steel sample with a carbon equivalent exceeding 0.065% in a 0.5 M NaCl solution. The theta plots indicate a phase angle peak of less than 90, suggesting non-ideal capacitive behavior in the tested sample and confirming the presence of system inhomogeneities. The modulus impedance, determined at the minimum frequency (R_{min}), is generally acknowledged to be correlated with corrosion resistance [20]. Nyquist plots for steel samples are shown in Figure 8. The variations of the modulus impedance at the minimum frequency (R_{min}) are shown in Figure 9, the sample subjected to isostatic flow control in 0.5 M NaCl demonstrates the highest corrosion resistance (highest R_{min}), while other parameters contribute to an acceleration in the corrosion rate.

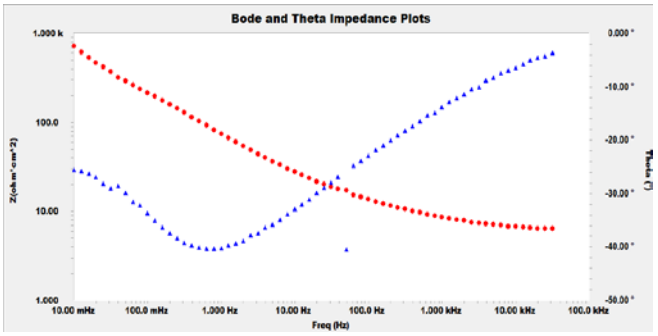

Figure 7. Bode and theta Impedance plots for the steel samples.

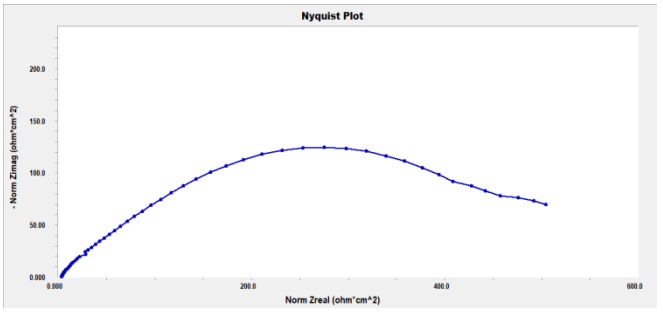

Figure 8. Nyquist plots for the steel samples.

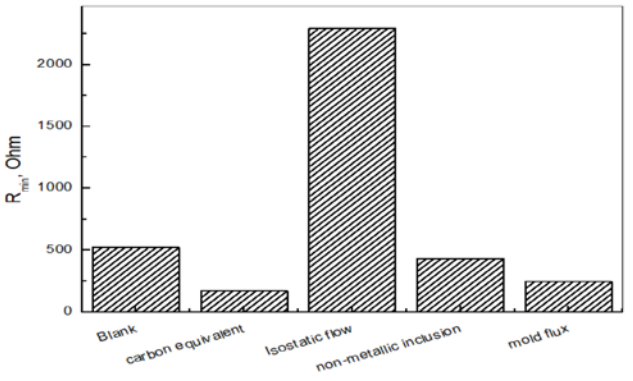

Figure 9. Variation of the modulus impedance at the minimum frequency (Rmin) determined from Bode impedance measurements of the tested samples in 0.5 M NaCl.

Table 3 : Electrochemical polarization parameters for different parameters of steel

Parameters	i_{corr} ($\mu A/cm^2$)	$-E_{corr}$ (mV)	β_a (mV/decade)	B_c (mV/decade)	Corrosion rate (mpy)
Blank without defect	5.44	649	84	110	1.6
Carbon equivalent > 0.06	45.32	667	85	910	13.9
Isostatic Flow Control (2.6 tone/minute)	4.76	704	138	196	1.4
Non-Metallic Inclusion	6.53	679	132	55	2.0
Mold Flux	8.12	688	87	87	2.4

3. Material and Method (Experimental and methodology work).

3.1 Solution Preparation.

The test solutions of 3.5% NaCl are prepared from analytical grade sodium chloride and distilled water.

3.2 Electrochemical Techniques.

Potentiodynamic and electrochemical impedance spectroscopy (EIS) measurements are being conducted by linking the electrochemical cell to a Gamry instrument. These measurements take place using the three-electrode mode of an electrochemical cell at the rest potential. As a reference electrode, a saturating calomel electrode (SCE) is employed, while a counter electrode is represented by a platinum sheet sealed in a ground joint. The working electrodes are fabricated from low-carbon, low-manganese aluminum-killed steel, with the chemical composition detailed in Table 4.

In the current procedure, the working electrodes are fashioned into rectangular plates and subsequently encapsulated with epoxy resin, leaving one side exposed for contact with the 3.5% NaCl solution, providing a surface area of 1.5 cm^2. Prior to utilization, the working electrode undergoes grinding with zirconia grit abrasive papers. Before initiating polarization and electrochemical impedance spectroscopy (EIS) measurements, the working electrode is allowed to achieve the open-circuit potential in the test solution for 20 minutes. In impedance measurements, 10 points are recorded for each decade of frequency within the range of 30 kHz to 0.01 Hz, with a superimposed AC potential amplitude of 10 mV. Polarization curve measurements are acquired at a scan rate of 1 mV, commencing from the cathodic potential (Ecorr -300 mV) and moving in the anodic direction. All measurements are conducted at 25 °C in solutions open to the atmosphere under unstirred conditions. To assess the reliability and reproducibility of the measurements, duplicate experiments are carried out under identical conditions in each case.

3.3 Metallographic Tests.

In the current methodology, small square samples with dimensions of 10.0 mm x 10.0 mm x 1.2 mm are extracted from low-carbon, low-manganese aluminum-killed steel using a metallographic wet cutter (CONRAD). Subsequent to sample preparation, SEM analysis is performed utilizing a JEOL JSM-6010LV model, accompanied by Energy Dispersive X-ray analysis (EDX) to identify the elemental composition of the cracked sample and ascertain the origin of the defect.

The upper surfaces of the samples, featuring longitudinal facial cracks, undergo grinding with 1000 silicon carbide abrasive grit papers, followed by polishing with emery paper, and finally, they are molded in Bakelite. Throughout the grinding and polishing processes, distilled water is employed.

4. Conclusion

The longitudinal facial crack (LFC) defect is observed at various locations along the width of the slab, exhibiting varying degrees of severity. Adjusting carbon equivalent values and fine-tuning mold flux properties has resulted in a reduction of the LFC index. To enhance product quality, attention is directed towards adjusting the Al/Ca ratio at the ladle metallurgy furnace (LMF) to fall within the specified range of 8-12. Electrochemical techniques have revealed that an isostatic flow parameter of 2.6 tons/minute effectively inhibits the corrosion of LFC samples. However, it is noteworthy that other parameters, including non-metallic inclusions, mold flux, and carbon equivalent, contribute to the induction of corrosion in the LFC defect.

5. Acknowledgment

We extend heartfelt thanks to all contributors to this research, particularly EZZ Dekhila Steel for essential resources along with the Institute of Graduate Studies and Research, for facilitating all laboratory resources.

6. Conflict of Interest

This research holds significant importance for the steel industry as it marks a pioneering approach by integrating electrochemical techniques with scanning electron microscopy for process enhancement. Notably, this innovative combination has been applied for the first time, signifying a groundbreaking advancement in the field. It is noteworthy that this research was conducted without external funding, and a mutual agreement with the company facilitated the exploration of this specific aspect, underscoring the collaborative nature of the study.

Table 4: Chemical composition of the low-carbon, low-manganese aluminum killed steel.

C	Si	Mn	P	S
0.049~0.063%	0.051~0.076%	0.122~0.201%	0.003~0.008%	0.001~0.008%
Ni	Cr	Cu	V	Nb
0.002~0.0030%	0.0018~0.0019%	0.005~0.006%	0.0001%	0.000~0.001%
Ti	Ca	B	Al	N_2
0.002~0.003%	0.0028~0.0035%	0.0002~0.003%	0.035~0.043%	40~50 ppm

References

[1] Bhattacharya, D.; Misra, S.; Kumar, A.; Mahashabde, V.V. Investigated the Root Cause Analysis of Surface Detection in Coils Produced Through Thin Slab Route. In 10th International Conference on Molten Slags, Fluxes, and Salts, 2016, 255-257.

[2] Peng, Q.; Zou, J.; Qiu,L.; Tong, Z.; Xiong,W. Investigation of Surface Longitudinal Crack on SPA-H Steel Slab by Compact Strip Production (CSP). Advanced Material Research, 2022, 190-196.

[3] Sun, Y.H.; Ni, Y.J.; Wang, H.T.; Xu, Z.B; Cai, K.K. Longitudinal Surface Cracks in Thin Slabs. The International Journal of Minerals, Metallurgy, and Materials, 2010, 17(2), 159-166.

[4] Hibbeler, L.C.; Thomas, B.G.; Santillana, B.; Hamoen,A.; Kamperman,A. Longitudinal Face Crack with Thermo-mechanical models of thin slab in Funnel molds. 6th European Continuous Casting Conf., Assoc. Italian Metallurgica, Ricionne, Italy, 2008, 1-15.

[5] Haiyang, D.; Wei, Jingjing; Qi, Lin; Wang, Xudong; Liu, Yu; Yao, Man. Longitudinal Crack Detection Approach Based on Principal Component Analysis and Support Vector Machine for Slab Continuous Casting. Steel Research Int., 2021, 2100168, 1-10.

[6] Ervasti, E.; StaÊhlberg, U. Behavior of Longitudinal Surface Cracks in the Hot Rolling of Steel Slabs. Department of Materials Processing, Royal Institute of Technology, Brinellvagen 23, Stockholm S-10044, Sweden,1999, 141-150.

[7] LIU, Y; WANG, X.; SUN, Y.; GAO, Y. Visual Detection Method of Longitudinal Crack Based on Computer Image Processing During Slab Continuous Casting. Arch. Metall. Mater. 2018, 63, 673-680.

[8] Fengming, D.; Xudong, W.; Yu, L.; Jingjing, W.; Man, Y. Prediction of Longitudinal Cracks Based on a Full-Scale Finite-Element Model Coupled Inverse Algorithm for a Continuously Cast Slab. WILEY-VCH Verlag GmbH & Co. KGaA, Weinheim, 2017, 1-7.

[9] Lee, Y.S.; Kim, S.; Won Jang, D.;Lee, S.B. Mechanism of Crack Initiation and Propagation in High-Alloy Steel Slabs during the Cooling and Scarfing Processes after the Continuous Casting Process. Mechanics of Materials. 2022, 104240, 1-10.

[10] Brimacombe, J.K.; Sorimachi, K. Crack Formation in the Continuous Casting of Steel. Metallurgical Transition B, 1977, 8, 489-505.

[11] Shabovta,V.P.; Torgovets, A.K.; Maksimov, E. V. Formation of Longitudinal Cracks on Slabs. 2010, 40, 558-561.

[12] Fogazzi, W.; De Souza, B.V. Ferrite Potential Influence on Heat Transfer Condition in Industrial Mold during the Continuous Casting of Steel. Engenharia Térmica Thermal Engineering, 2018, 18-23.

[13] Harmuth, H.; Xia, G. Interaction. Steel/Slag/Submerged Entry Nozzle and its Impact on Refractory Wear Thermochemical Process Simulation. ISIJ International, 2015, 55, 775–778.

[14] Rackers, K.G.; Thomas, B.G. Clogging in Continuous Casting Nozzles.78th Steelmaking Conference Proceedings, Nashville, TN, 1995, 723-734.

[15] Alan, W. C.; Ravi Rastogi.; Roger, L. M. Nozzle Clogging. The AISE Steel Foundation, Pittsburgh, PA. 2003, 1-4.

[16] Zhang, L.; Thomas, B.G. Inclusion in Continuous Casting of Steel. XXIV National Steelmaking Symposium, Morelia, Mich, Mexico, 26-28 Nov. 2003, 138-183.

[17] V. Rusňáková; J. Kijac; G. Grimplini; G. Rusňák; Louis Pasteur. Analysis of Slag in Mold Under Standard Conditions and in Case of Sticker Temperature Alarm Occurrence. Acta Metallurgica, Slovakia, 2010, 16, 172-179.

[18] Kenneth, C. Mills. Mold Powder for Continuous Casting. The AISE Steel Foundation, Pittsburgh, PA, 2002, 10-16.

[19] Billany, T.J.H.; Mills, K.C. Mold Flux Performance during continuous casting. the Commission of the European Communities, 1988, 1-19.

[20] Abdel-Gaber, A.M.; Najem A.; Awad R. The Electrochemical Corrosion Behavior of Compacted (Bi, Pb)-2223 Superconductors in Aqueous Solutions. Sci Rep. 2022, 12, 17941; doi: 10.1038/s41598-022-22663-6.

[21] Kenneth C. Mills; Carl-Åke Däcker. The Casting Powder Book. Springer International Publishing, 2017, 321-324.

[22] Y. LIU; X. WANG; Y. SUN; Y. GAO. Visual Detection Method of Longitudinal Crack Based on Computer Image Processing During Slab Continuous Casting. Metall Mater. 2018, 63, 673-680.

[23] Y.H. Sun; Y.J. Ni; H.T. Wang; Z.B. Xu; K.K. Cai. Longitudinal Surface Cracks in Thin Slabs. the International Journal of Minerals, Metallurgy, and Materials, 2010, 17 (2), 159-166.

[24] Rusňáková, V.; Kijac, J.; Grimplini, G.; Rusňák, G.; Louis Pasteur. Analysis of Slag in Mold Under Standard Conditions and in Case of Sticker Temperature Alarm Occurrence. Acta Metallurgica, Slovakia, 2010, 16, 172-179.